The Kinematics of Bi-polar HII Regions

OPAL Australia Telescope Compact Array Cover Sheet v.2.1

Proposal Details

Instrument	Australia Telescope Compact Array
Title	The Kinematics of Bi-polar HII Regions
Type	Standard
Proposal submitted in previous semester	No
Pre-graded status	No
Science keywords	ISM, interstellar medium in and around the Milky Way, spectral line (Galactic), star formation (Galactic)
Other science keywords	
Qualified observer will be present	Yes
Used for PhD thesis	No

Investigators

Name	Affiliation	Email	PhD Student	Expert
Principal Investigator				
Wenger, Trey	University of Wisconsin	twenger2@wisc.edu	No	Yes
Co-Investigators				
Bonne, Lars	NASA Ames Research Center	lbonne@usra.edu	No	No
Emig, Kimberly	National Radio Astronomy Observatory	kemig@nrao.edu	No	No
Salas, pedro	Pontificia Universidad Catolica de Chile	salas.mz@gmail.com	No	No

Observing Experts

ATNF expert requested	No

Nominated observing experts are indicated in the Investigators table above.

ATCA Setup

Consulted archives	Yes
Other information	['Imaging']

Abstracts

Science Abstract

Understanding the dynamics and evolution of HII regions and their surroundings provides essential constraints on models of both the high-mass star formation process as well as the subsequent impact on the surrounding interstellar medium (ISM). Bi-polar HII regions, although relatively rare, play a critical role in shaping the ISM in their vicinity. Recent high-angular resolution [CII] observations reveal a complex kinematic environment in the photo-dissociation regions surrounding some bi-polar HII regions. On the other hand, a recent RRL survey of HII regions discovered that many nebulae show organized ionized gas velocity fields. We propose to observe RRL and radio continuum emission at high angular resolution toward five nearby bi-polar HII regions in order to relate the ionized gas kinematics to that of the surrounding neutral and molecular material. We will also observe one unique and mysterious bi-polar HII region to elucidate its nature. We will use existing ATCA RRL data, as well as auxiliary molecular and neutral gas data, to compliment these observations, which will reveal the nature of bi-polar HII regions and their impact on the ISM.

Outreach Statement

Massive stars -- those that are 20 or more times more massive than the Sun -- have a significant impact on their surroundings. These stars emit intense radiation, which drives energy into the interstellar matter. This disruption can drive the formation of even more stars, or it can prevent other stars from forming. By understanding the physical mechanisms that help to propogate this energy into interstellar space, we will learn more about how massive stars shape galaxies like our own Milky Way. We are using the Australia Telescope Compact Array to search for faint radio waves associated with the hot gas surrounding these young massive stars. These data will show us how the ionized gas is moving around within the star forming region and help us understand how energy is transported into and out of the nebulae.

Schedule

Total Time Required	275 hours
Time Allocated	0 hours

OPAL Australia Telescope Compact Array Observations Table v.2.0

Warning: Observation table coordinates may be truncated in hardcopy PDFs.

Name	Position		LST Range		Integration Time per Day (Hours)	Number of Epochs	Total Time (Hours)	Target type	Angular size (Arcsec)	Array config.	Band (one or more)	CABB observing mode	Peak flux (mJy)	Transitions
	Glong	Glat	Start	End										
W40	28.79	3.48	13:22	23:40	1	1	1.0	single source	600	H75	4cm	CFB 64M-32k	80	Several RRLs
W40	28.79	3.48	13:22	23:40	2	1	2.0	single source	600	H168	4cm	CFB 64M-32k	80	Several RRLs
W40	28.79	3.48	13:22	23:40	3.5	1	3.5	single source	600	H214	4cm	CFB 64M-32k	80	Several RRLs
W40	28.79	3.48	13:22	23:40	3.5	2	7.0	single source	600	EW367	4cm	CFB 64M-32k	80	Several RRLs
W40	28.79	3.48	13:22	23:40	3.5	4	14.0	single source	600	Any750m	4cm	CFB 64M-32k	80	Several RRLs
W40	28.79	3.48	13:22	23:40	7	4	28.0	single source	600	Any1.5km	4cm	CFB 64M-32k	80	Several RRLs
RCW 36	265.07	1.40	2:06	15:51	3.5	1	3.5	single source	400	H214	4cm	CFB 64M-32k	180	Several RRLs
RCW 36	265.07	1.40	2:06	15:51	3.5	2	7.0	single source	400	EW367	4cm	CFB 64M-32k	180	Several RRLs
RCW 36	265.07	1.40	2:06	15:51	3	4	12.0	single source	400	Any750m	4cm	CFB 64M-32k	180	Several RRLs
RCW 36	265.07	1.40	2:06	15:51	7	4	28.0	single source	400	Any1.5km	4cm	CFB 64M-32k	180	Several RRLs
G316.80–00.05	316.80	-0.04	6:38	22:52	3.5	1	3.5	single source	300	H214	4cm	CFB 64M-32k	360	Several RRLs
G316.80–00.05	316.80	-0.04	6:38	22:52	3.5	2	7.0	single source	300	EW367	4cm	CFB 64M-32k	360	Several RRLs
G316.80–00.05	316.80	-0.04	6:38	22:52	3	4	12.0	single source	300	Any750m	4cm	CFB 64M-32k	360	Several RRLs
G316.80–00.05	316.80	-0.04	6:38	22:52	7	4	28.0	single source	300	Any1.5km	4cm	CFB 64M-32k	360	Several RRLs
G319.88+00.79	319.88	0.77	7:10	22:56	3.5	1	3.5	single source	200	H214	4cm	CFB 64M-32k	60	Several RRLs
G319.88+00.79	319.88	0.77	7:10	22:56	3.5	2	7.0	single source	200	EW367	4cm	CFB 64M-32k	60	Several RRLs
G319.88+00.79	319.88	0.77	7:10	22:56	3.5	4	14.0	single source	200	Any750m	4cm	CFB 64M-32k	60	Several RRLs

G319.88+00.79	319.88	0.77	7:10	22:56	7	4	28.0	single source	200	Any1.5km	4cm	CFB 64M-32k	60	Several RRLs
G330.04–00.06	330.04	-0.06	8:39	23:30	3.5	1	3.5	single source	140	H214	4cm	CFB 64M-32k	40	Several RRLs
G330.04–00.06	330.04	-0.06	8:39	23:30	3.5	2	7.0	single source	140	EW367	4cm	CFB 64M-32k	40	Several RRLs
G330.04–00.06	330.04	-0.06	8:39	23:30	3.5	4	14.0	single source	140	Any750m	4cm	CFB 64M-32k	40	Several RRLs
G330.04–00.06	330.04	-0.06	8:39	23:30	7	4	28.0	single source	140	Any1.5km	4cm	CFB 64M-32k	40	Several RRLs
G345.88–01.10	345.88	-1.10	10:27	23:56	1	1	1.0	single source	60	H75	4cm	CFB 64M-32k	3	Several RRLs
G345.88–01.10	345.88	-1.10	10:27	23:56	2	1	2.0	single source	60	H168	4cm	CFB 64M-32k	3	Several RRLs
G345.88–01.10	345.88	-1.10	10:27	23:56	3.5	1	3.5	single source	60	H214	4cm	CFB 64M-32k	3	Several RRLs
G345.88–01.10	345.88	-1.10	10:27	23:56	3.5	2	7.0	single source	60	EW367	4cm	CFB 64M-32k	3	Several RRLs

Total time for semester: 275.0

THE KINEMATICS OF BI-POLAR H II REGIONS

Background. H II regions are the volumes of ionized gas that surround recently-formed OB-type stars. Feedback from these massive stars injects significant energy into the surrounding interstellar medium (ISM), which may trigger or inhibit star formation[1] and drive turbulence[5]. The internal kinematics of H II regions constrain models of both early-time high-mass star formation and angular momentum transportation as well as late-time feedback injection into the ISM. At early times, the accretion of natal material[10] or other mechanisms that affect the inheritance of angular momentum from the parent molecular cloud[8] may be important in the formation and early evolution of high-mass stars and their surroundings. At later times, the interaction between the ionized volume and the surrounding neutral and molecular medium affects the total energy input into the ISM[9]. Observations that probe the kinematics of the ionized gas, photo-dissociation region (PDR), and nearby neutral and molecular gas associated with H II regions are needed to create a comprehensive picture of high-mass star formation and stellar feedback.

Radio recombination lines (RRLs) are an unobscured tracer of ionized gas kinematics in and around Galactic H II regions. For example, a recent ATCA RRL survey of Milky Way H II regions at a resolution of $\sim$1.5′ discovered a previously-unknown population of nebulae with ionized gas velocity gradients [3]. Of the $\sim$100 nebulae with sufficient sensitivity to spatially resolve the RRL emission, $\sim$50% have a clear RRL velocity gradient. The mechanism that drives these velocity gradients remains a mystery, however, due to the poor angular resolution of the original survey. Preliminary results from a follow-up, higher angular resolution ($\sim$15″) survey of a subset of these nebulae reveals a kinematically complicated environment within the ionized volumes of H II regions (see Figure 1).

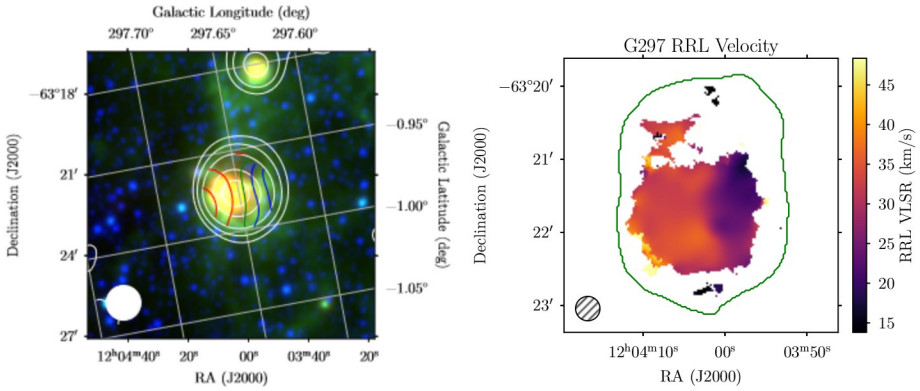

Figure 1: The ionized gas kinematics of G297.651−00.973. The left panel is a three-color composite from the *WISE* All-Sky Survey (3.4 μm in blue, 12 μm in green, and 22 μm in red), with white radio continuum contours at 5, 10, 20, 50, and 80% of the peak continuum brightness, and hydrogen RRL LSR velocity contours ranging from -35km s^{-1} (blue) to -27km s^{-1} (red). The radio data come from the original low-resolution ATCA survey. The right panel shows the hydrogen RRL LSR velocity field with preliminary data from the $\sim$15″ follow-up ATCA survey. With better resolution, the kinematic structure of the ionized gas appears to be more complicated than just a simple gradient.

Bi-polar H II regions represent a relatively rare subset ($<$5%[11]) of the Galactic H II region population, yet their complex expansion dynamics play a critical role in shaping the surrounding ISM [7]. The limited models of bi-polar H II regions predict that these nebulae exist in a relatively long-lived morphological phase [4, 13, 15]. A recent investigation of [C II] emission at 158 μm associated with the PDR of the H II region RCW 36, however, suggests that bi-polar morphologies may be a much shorter phase ($\sim$0.2 Myr) in H II region evolution due to the complicated and anisotropic expansion dynamics of the PDR material [7].

Scientific Justification. The origin of ionized gas velocity gradients in bi-polar H II regions, along with the relationship between the kinematics of the ionized gas and the surrounding material, are two primary uncertainties in our understanding of the early stages of massive star formation and its feedback on the ISM[8]. We propose to resolve these mysteries by answering the following questions:

1. **What are the kinematics and physical conditions of the ionized gas associated with bi-polar H II regions?** Understanding the internal conditions (e.g., excitation conditions, emission measure, dynamics) of these nebulae, including spatial variations across the core and lobes of emission, is essential for a comparison with bi-polar H II region evolutionary models [7].
2. **Is there a preferred orientation of ionized gas velocity gradients in bi-polar H II regions?** Of the few nebulae with sufficient angular resolution to resolve the kinematic structure of the ionized gas, most demonstrate ionized gas

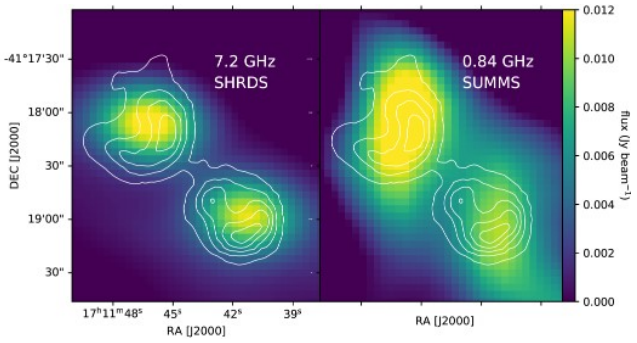

Figure 2: Radio continuum emission at 0.84 and 7.2 GHz toward the G345.88−01.10, showing a clear bipolar morphology. The massive infrared-dark clump is located in the middle of the two lobes.

velocity gradients perpendicular to the bi-polar axis [3, 8], although there is evidence for more complicated scenarios [2].

3. **How do the ionized gas kinematics of bi-polar H II regions differ from other morphological classes?** Bi-polar H II regions may have more anisotropic internal kinematics that mimic the [C II] PDR kinematics [7], or they may tend to be more ordered if their kinematics are dominated by rotation [8]. We must understand the mechanisms at play in order to quantify the importance of feedback from these nebulae.
4. **What is the relationship between the ionized gas kinematics and the kinematics of the surrounding PDR?** For example, do the anisotropies in the [C II] velocity field of the PDR match anisotropies in the ionized gas velocity field within the H II region? If so, then we will be able to constrain the energy transport through the nebula and into the ISM, but, if not, then we will need to explore other possible explanations for the [7] observational result.
5. **What is the nature of G345.88−1.10?** Our final motivating question relates to a single, mysterious object. A recent kinematic analysis of this star forming complex with an apparent bi-polar morphology suggests that the massive 70 μm-dark clump between the bipolar infrared- and radio-bright nebulosities represents a new, early stage of massive star formation [6] (see Figure 2). The recent detection of RRLs toward this nebulosity, however, suggests that this object is simply a faint, bi-polar H II region [14]. A deeper and higher angular resolution map of RRL emission will elucidate the nature of the object and its relationship to the infrared-dark clump. For example, the detection of an ionized gas velocity gradient along the bi-polar axis would suggest that the nebulosities are indeed being driven by *something* hiding within or near to the clump.

Name	ℓ	b	Distance	T_L
	deg	deg	kpc	mK
W40	28.79	3.48	0.4	800
RCW 36†	265.07	1.40	0.95	1800
G316.80−00.05†	316.80	-0.04	2.8	3600
G319.88+00.79†	319.88	0.77	2.6	600
G330.04−00.06†	330.04	-0.06	2.6	400
G345.88−01.10†	345.88	-1.10	2.3	30

Table 1: Proposed bi-polar H II region targets, their Galactic positions, distance estimates, and expected hydrogen RRL brightness temperatures at 6 GHz, T_L. Targets identified by a dagger (†) already have the necessary H75 and H168 data from a previous project (C2963).

Proposed Observations. We propose to observe C/X-band (4–10 GHz) radio continuum and RRL emission at high angular resolution toward a sample of five bright, nearby bi-polar H II regions identified by [11] and the FEEDBACK legacy program [12], as well as G345.88−1.10 (see Table 1). These targets are selected based on their expected brightness and available auxiliary data products: two nebulae (W40 and RCW 36) have [C II] observations at ∼15″ resolution, G345.88−01.10 has a variety of molecular gas observations [6], and all of the nebulae have archival infrared and radio continuum images. A subset of our targets (indicated by a dagger in Table 1) already have some low-angular resolution RRL observations from a previous project (C2963).

We will use the continuum and hydrogen RRL data to derive the physical conditions of the gas, such as the rms electron density, electron temperature, emission measure, and the rate of photoionization by the ionizing sources, with sufficient angular resolution and sensitivity to search for spatial variations. This sample of six nebulae, along with an additional source from an associated project (C3410), will allow us to determine the typical conditions and variety of conditions in the bi-polar

H II region population, which will place direct constraints on models (Question 1). These high-angular resolution RRL observations will also allow us to map the kinematics of the ionized gas across the nebulae in order to correlate the orientation of ionized gas velocity gradients with their bi-polar axes as seen in the mid-infrared (Question 2, see Figure 1). Our observing procedure matches that of the associated project C3410 (see Figure 1), so we will be able to contrast the inferred internal kinematics of these bi-polar H II region observations against a sample of H II regions of various morphologies (Question 3).

A subset of our proposed targets have [C II] observations from the Stratospheric Observatory for Infrared Astronomy (SOFIA) FEEDBACK C^+ Legacy survey [12]. Our proposed observations of these targets will match the $\sim$15″ SOFIA resolution. We will directly compare the kinematics of the ionized gas to the PDR material traced by [C II] in order to test the model of kinematic anisotropies in PDRs around bi-polar H II regions [7] (Question 4). Furthermore, carbon RRLs, which we will detect towards the brightest targets, are an unobscured tracer of the PDR closer to the molecular boundary layer and thus complement the [C II] data.

Finally, we will observe the much fainter source, G345.88−01.10, to better understand its nature (Question 5). We will not be able to achieve the same angular resolution due to the faintness of the RRL emission, but by combining some deeper short-baseline and longer-baseline observations with the C2963 data, we will search for ionized gas velocity gradients and correlations with other molecular gas tracers[6].

Technical Justification and Feasibility. The ATCA with CABB is the ideal instrument for deep RRL observations of Galactic H II regions. The compact antenna configurations provide the surface brightness sensitivity required to map the faint RRL emission, and the wide bandwidth C/X-band receiver and flexible correlator can observe $\sim$20 RRL transitions simultaneously. By stacking the different RRL spectra, we increase our signal-to-noise ratio significantly. Since we will combine these new data with existing H75 and H168 data, we will use the same CABB configuration as used by previous projects (C2963). The spectral resolution of $\sim$1km s^{-1} is sufficient to spectrally resolve both the broad (FWHM $\simeq$30km s^{-1}) hydrogen RRLs and narrow (FWHM $\simeq$few km s^{-1}) carbon RRLs.

For all of our targets except G345.88−01.10, we aim to map the RRL emission at an angular resolution matching that of the SOFIA [C II] observations ($\sim$15″). The resolution of the 1.5 km array configuration at our lowest frequency RRL transition is $\sim$12″ and meets our objective. The remaining target, G345.88−01.10, was resolved by C2963 in the H168 antenna configuration, but without sufficient sensitivity to search for ionized gas velocity gradients. We will therefore observe this source deeper with the same H75 and H168 configurations as in C2963, and also add EW367 to improve the angular resolution.

We estimate the expected brightness of the RRL emission based on previous RRL observations listed in Table 1. These previous observations come from low angular resolution observations and thus the RRL brightness in our proposed high-angular resolution observations will depend on the emission structure. The radio continuum emission from these nebulae is sufficiently compact to fit within the ATCA primary beam at our highest frequency RRL transition. For our faintest target (excluding G345.88−01.10), we require an rms sensitivity of $\sim$20mK in the stacked RRL spectrum in order to achieve a signal-to-noise ratio of $\sim$20 based on the previous observations. There will likely be more compact, higher-brightness structures in our high-angular resolution observations, so this sensitivity should be sufficient to map RRL emission across the nebulae. Furthermore, this sensitivity will allow us to detect carbon RRLs, which are typically 10$\times$ fainter than hydrogen RRLs, toward the two or three brightest targets. Based on experience in previous projects, we will be able to stack $\sim$18 RRL transitions, so our target spectral rms is 80mK. According to the ATCA sensitivity calculator, we require $\sim$40min of on-source time in the H75 configuration, which is consistent with previous experience.

Based on preliminary results from the related project C3410, we require a factor of $\sim$2 more integration time in each successively larger antenna configuration in order to create high-dynamic range images of the RRL emission. Accounting for the H75 and H168 data already observed, but including the additional deeper observations needed for G345.88−01.10, we require a total on-source time of 1.5 hr in H75, 3 hr in H168, 16 hr in H214, 32 hr in EW367, 53.5 hr in 750 m, and 107 hr in 1.5 km. The total on-source time request is 211.5 hr. Including a 30% calibration overhead, our total time request is 275 hr.

References. [1] Ali, A., Harries, T. J., & Douglas, T. A. 2018, MNRAS, 477, 5422; [2] Balser, D. S., Goss, W. M., & De Pree, C. G. 2001, AJ, 121, 371; [3] Balser, D. S., Wenger, T. V., Anderson, L. D., et al. 2021, ApJ, 921, 176; [4] Bodenheimer, P., Tenorio-Tagle, G., & Yorke, H. W. 1979, ApJ, 233, 85; [5] Boneberg, D. M., Dale, J. E., Girichidis, P., & Ercolano, B. 2015, MNRAS, 447, 1341; [6] Bonne, L., Peretto, N., Duarte-Cabral, A., et al. 2022, A&A, 665, A22; [7] Bonne, L., Schneider, N., Garcia, P., et al. 2022, ApJ, 935, 171; [8] Dalgleish, H. S., Longmore, S. N., Peters, T., et al. 2018, MNRAS, 478, 3530; [9] Gendelev, L., & Krumholz, M. R. 2012, ApJ, 745, 158; [10] Keto, E., & Wood, K. 2006, ApJ, 637, 850; [11] Samal, M. R., Deharveng, L., Zavagno, A., et al. 2018, A&A, 617, A67; [12] Schneider, N., Simon, R., Guevara, C., et al. 2020, PASP, 132, 104301; [13] Wareing, C. J., Pittard, J. M., & Falle, S. A. E. G. 2017, MNRAS, 465, 2757; [14] Wenger, T. V., Dawson, J. R., Dickey, J. M., et al. 2021, ApJS, 254, 36; [15] Whitworth, A. P., Priestley, F. D., & Geen, S. T. 2022, MNRAS, 517, 4940